In Situ Growth of MnO_2 on pDA-Templated Cotton Fabric for Degradation of Formaldehyde

Yali Zhang
Wuhan Textile University
Zhong Zhao
Wuhan Textile University
Daiqi Li
Wuhan Textile University
Guangming Cai
Wuhan Textile University
Xiaoning Tang
Wuhan Textile University
Wenbin Li
Wuhan Textile University
Deshan Cheng (chengcds@163.com)
Wuhan Textile University https://orcid.org/0000-0002-4504-7473
Xin Wang
Wuhan Textile University

Research Article

Keywords: MnO2 NPs, cotton fabric, pDA, HCHO, removalefficiency

Posted Date: December 29th, 2021

DOI: https://doi.org/10.21203/rs.3.rs-1134182/v1

Abstract

Degradation of formaldehyde (HCHO) in interior decoration has been an urgent issue due to its toxicity nature and potential threats to human health. In this work, manganese dioxide nanoparticles (MnO_2 NPs) were in situ grown on the polydopamine (pDA)-templated cotton fabrics for environmentally friendly HCHO degradation applications. The morphology, elemental composition, and crystal structure of the cotton/pDA/MnO_2 were characterized by scanning electron microscopy-energy dispersive X-ray spectrum (SEM-EDX), Fourier transform infrared (FT-IR), X-ray diffractometer (XRD) and X-ray photoelectron spectroscopy (XPS), respectively. The degradation of HCHO by the as-developed cotton/pDA/MnO_2 was measured in a self-made quartz reactor, and the stability of adsorption was evaluated by cyclic experiments. The results showed that the HCHO removal efficiency reached to 100% within 20 min after three cycles, suggesting that the as-prepared fabrics exhibited good stability for the degradation of HCHO. The development of MnO_2 NPs coated fabrics provides new strategies in degradation HCHO in interior decoration.

1. Introduction

Decorative materials, furniture boards and building materials are widely used in interior decoration, resulting in an inevitable problem of indoor formaldehyde (HCHO) pollution. Long-term exposure to HCHO may cause serious harm to human respiratory tract, skin diseases and nervous system, and even increased incidence of cancer (Kim et al. 2011; Inci et al. 2013; Abdu et al. 2014). Therefore, it is of great significance to develop efficient and stable HCHO scavenging technology for indoor air purification. At present, physical adsorption (Chen et al. 2017a; Falco et al. 2018), green planting (Chen et al. 2017b), ozone (Zhu et al. 2017a) and catalytic oxidation (Quiroz et al. 2013; Nie et al. 2016; Bai et al. 2016) are the widely applied methods to remove HCHO. Physical adsorption method is simple and easy to perform, but the performance of the adsorbent is not stable with issues of adsorption saturation and secondary pollution. Green planting can decompose HCHO by photosynthesis, but its removal efficiency is low and there is no adsorption efficacy when dealing with high concentrations of HCHO. Ozone's effect on HCHO is only limited to that in air state but not to the pollution source. In the catalytic oxidation method, HCHO is firstly oxidized to formic acid under the action of catalyst followed by conversion into nontoxic CO_2 and H_2O. Among these methods, catalytic oxidation has the advantages of simple operation, high conversion efficiency and no secondary pollution, demonstrating itself to be the most effective method in removal of indoor HCHO pollution.

Manganese dioxide (MnO_2) as a transition metal oxide is an efficient catalyst for the catalytic oxidation of HCHO due to its low-cost, abundant surface hydroxyl groups and variable manganese valence (Rong et al. 2018; Wang et al. 2019; Dai et al. 2020; Ji et al. 2020). Zhu et al. (2017b) reported that Ce-modified MnO_2 showed great activity for HCHO oxidation at a low temperature. Wang et al. (2017) designed layered-structure MnO_2 with different amounts of manganese vacancy for catalytic oxidation of HCHO. Lu et al. (2016) fabricated graphene-MnO_2 hybrid nanostructure as a new catalyst for HCHO oxidation.

Although several highly active MnO_2 catalysts have been successfully synthesized, they cannot be used directly for practical applications. The reason for this is mainly due to the powder form of MnO_2 catalysts, and a carrier is usually needed to support them for subsequent catalytic oxidation. Therefore, how to expose the active sites of the catalysts to maintain its high activity and stability is still a great challenge.

In this work, MnO_2 NPs were synthesized on pDA-templated cotton fabrics via a facile hydrothermal route. Due to the abundant catechol functional groups of pDA which can chelate with Mn metal ions, the MnO_2 nanoparticles were uniformly dispersed on the surface of cotton fibers. The MnO_2-loaded fabrics had rich porosity and highly exposed active sites, leading to a thorough and quick conversion of HCHO into CO_2 under light conditions. The stability of the MnO_2-loaded fabrics in HCHO removal was evaluated by performing repeated adsorption-degradation cycles. The possible reaction mechanism of HCHO removal by MnO_2-loaded fabric was also explored.

2. Experimental

2.1 Materials

Cotton fabrics with a density of 135 g/m^2 were supplied by Wuhan Yudahua Textile Co., Ltd (Wuhan, China). Hydroxytyramine hydrochloride (dopamine hydrochloride) was provided by Aldrich Chemical Co. (Milwaukee, USA). Potassium permanganate ($KMnO_4$), tris(hydroxymethyl) aminomethane (Tris), sodium hydroxide (NaOH) and acetone were purchased from Aladdin Chemical Co., Ltd (Shanghai, China).

2.2 Preparation

MnO_2 NPs coated cotton fabrics was fabricated by *in situ* growth method, as shown the preparation process in Fig. 1. Initially, cotton fabrics were immersed into a freshly dopamine solution (2 mg/mL, pH = 8.5) in an overhead shaker at 30 rpm. After self-polymerization for 24 h, the fabrics were washed with deionized water followed by drying at 60°C. The pDA-modified cotton fabrics are coded as cotton/pDA.

Secondly, the cotton/pDA was added into a $KMnO_4$ solution (50 mM, 100 mL) under shaking at 80°C for 8 h. After that, the fabrics were washed with deionized water and dried. The obtained cotton fabrics are coded as cotton/pDA/MnO_2.

2.3 Characterization and measurements

The morphology of the coated fabrics was characterized by scanning electron microscopy (SEM) (JSM-5600LV, JEOL, Japan) with an energy dispersive X-ray spectrum (EDX, Oxford Instruments, Oxford, UK). Fourier transform Infrared (FT-IR) spectra were measured using a TENSOR 27 FT-IR spectrometer (Bruker, Germany). The crystal structure of the fabrics was examined on an X-ray diffractometer (D/max 2500, Rigaku, Japan) using Cu Kα radiation in the 2θ range of 10-80°. The elemental composition of the cotton/pDA/MnO_2 was analysed by X-ray photoelectron spectroscopy using a Mg Kα source at 14.0 kV

and 25 mA (PHI-5000C ESCA, America). Thermogravimetry analysis was recorded on a thermal analyzer with a heating rate of 10°C/min from 30°C to 700°C under nitrogen atmosphere (Netzsch TG209 F1, Germany).

2.4 HCHO adsorption test

The HCHO adsorption test of the as-prepared fabrics was carried out in a self-made quartz reactor (Fig. 2). The cotton/pDA/MnO_2 was cut into 10×10 cm^2 pieces and suspend in the center of the reactor. Then, HCHO vapor was quickly introduced into the reactor by heating a 1 mL HCHO solution (38 wt%). After 2 min, the HCHO solution was absolutely volatized at 90°C with a stable concentration of HCHO vapor at 22.7 ppm. The concentrations of HCHO and CO_2 in the reactor were monitored in real time by respective detectors mounted on the upper panel of the reactor.

The stability of the as-prepared fabrics in removal of HCHO was evaluated by performing repeated adsorption-degradation cycles. Before each HCHO adsorption test, the adsorbed fabrics were exposed to light source for 3 h to ensure an thorough oxidization of HCHO into CO_2. The removal efficiency (E) of HCHO was evaluated according to the following Equation:

$$E = \frac{C_0 - C}{C_0} * 100\ \% \quad (1)$$

where C_0 and C are corresponding to the initial and current concentration of HCHO, respectively.

3. Result And Discussion

3.1 Characterization of cotton/pDA/MnO_2

The morphology of the pristine cotton, pDA coated cotton, and cotton/pDA/MnO_2 were detected by a scanning electron microscope. It can be seen from Fig. 3a that untreated pristine cotton exhibits a smooth surface, and the ribbon-like profile of cotton fibers are clearly observed. In Fig. 3b, the deposition and polymerization of dopamine has resulted in a rough surface of the fibers. The evenly distributed nanoparticles can be observed from Fig. 3c, and this is due to the incorporation of MnO_2 into the deposited pDA film on cotton fibers. In the SEM image captured under a high magnification (Fig. 3d), MnO_2 NPs are densely deposited on the surface of the cotton fibers without obvious aggregations. After the *in situ* growth process, the color of the cotton/pDA sample shifted from brown to black due to the loading of MnO_2 NPs (Insets of Fig. 3).

The EDX mapping (Fig. 3e) and spectrum (Fig. 3f) of the cotton/pDA/MnO_2 show four peaks for carbon (C), oxygen (O), manganese (Mn) and potassium (K) elements with the weight percentage of 22.26%, 54.78%, 18.91% and 4.05%, respectively. The high content of Mn element indicates that large amounts of MnO_2 NPs have been anchored onto the fabric surface. The dense loading of MnO_2 NPs is due to the abundant phenolic hydroxyl groups of pDA through chelation effects, which promotes the uniform growth

of MnO_2 NPs in the pDA film. These SEM and EDS results demonstrate that MnO_2 NPs have been uniformly dispersed on the surface of cotton fabrics.

The chemical structures of the pristine and nanocomposite deposited cotton fabrics were characterized by FTIR spectroscopy in the spectral ranges of 400 to 4000 cm^{-1}. The FT-IR spectra are shown in Fig. 4a. It can be observed that pristine cotton exhibits an obvious wide peak at 3330 cm^{-1} arising from –OH stretching vibration in hydroxyl groups. The peak at 2900 cm^{-1} corresponds to –CH bending absorption bands in methylene groups. The peaks at 1720 cm^{-1} and 1435 cm^{-1} are assigned to C=O stretching vibration and $–CH_2$ bending vibration, respectively. The peaks at 1330 cm^{-1} and 1030 cm^{-1} are resulted from O–H in-plane deformation vibration and C–O stretching vibration, respectively (Ran et al. 2021; Cheng et al. 2021). Similar characteristic peaks are appeared in the FTIR pattern of cotton/pDA. Besides, the extra peak at 1660 cm^{-1} is due to the stretching vibration effects of benzene ring groups, which can be attributed to the polymerization of dopamine on cotton surface (Ran et al. 2019). In addition, the intensity of the absorption peak at 3330 cm^{-1} is stronger than the original cotton, which is mainly due to the increase of reactive OH groups on the fiber surface after modification with dopamine. After MnO_2 is anchored on the surface of cotton fibers, the pristine characteristic peaks of cotton have been obviously weakened, and the characteristic peak for MnO_2 appears. For example, the peak (725 cm^{-1}) detected below 800 cm^{-1} is attributed to metal-oxygen (Mn–O) stretching (Li et al. 2011). These results have confirmed the successful modification of cotton substrate through pDA templating and MnO_2 nanocomposite deposition.

The crystalline structure of the different cotton samples was investigated by XRD (Fig. 4b-c). In Fig. 4b, the pristine cotton exhibits four obvious diffraction peaks at 2θ angle of 14.1°, 16.5°, 22.5° and 34.2°, which are attributed to the crystal faces (1-10), (110), (200), and (004) of cellulose Iβ, respectively (French et al. 2013; French 2014; Cheng et al. 2018). The cotton/pDA fabrics present a similar XRD pattern to pristine cotton, suggesting the negligible effects of the pDA layer on the crystalline structure of cotton. According to reported studies, this is mainly due to the amorphous structure of pDA (Wang et al. 2018; Cheng et al. 2020). With respect to cotton/pDA/MnO_2 (Fig. 4c), the characteristic peak intensity of pristine cotton phase is decreased, which is possibly due to the growing of MnO_2 NPs on the surface of cotton fabrics. Furthermore, four extra diffraction peaks at 2θ = 12.1°, 24.8°, 36.6° and 65.4° corresponding to the characteristic peaks (001), (002), (006) and (119) crystal planes of δ-MnO_2 (JCPDS No. 18-0802), respectively can be observed (Ma et al. 2019; Zhang et al. 2019). The XRD results proved the presence of δ-MnO_2 NPs on the surface of cotton fabrics.

The surface chemical state of the as-prepared samples was further investigated by XPS. The XPS wide scan spectrum of cotton/pDA/MnO_2 proved the presence of C, O, Mn, and K elements on the cotton/pDA/MnO_2 (Fig. 5a). The K element is from the reactant $KMnO_4$, which is in good agreement with EDX results. The high resolution C1s spectrum in Fig. 5b can be deconvoluted into three peaks at 288.1 eV, 286.2 eV and 284.8 eV corresponding to the C=O, C-O/C-H, C-C bonds, respectively (Qi et al. 2021). Mn

2p XPS core level spectrum is shown in Fig. 5c, in which two peaks at 653.7 eV and 642.2 eV are attributed to Mn2p 1/2 and Mn2p 3/2 of Mn^{4+}, respectively (Miao et al. 2021). Additionally, the spin-energy separation of 11.5 eV has agreed well with previously measured spectra of MnO_2 (Lu et al. 2017; Shi et al. 2018). The O1s spectrum can be fitted into three peaks at 533.7 eV, 531.5 eV, 529.7 eV, which are attributed to C-O/C=O, Mn-O-H, and Mn-O-Mn, respectively (Fig. 5d) (Wang et al. 2016). XPS analysis indicated that MnO_2 NPs were successfully coated on the cotton fabric surface by in-situ growth.

3.2 Thermal properties

The thermal properties of cotton, cotton/pDA, and cotton/pDA/MnO_2 were characterized by TG analysis, as shown in Fig. 6. It can be observed that the residual weight of all samples exhibited a slight decrease in the initial stage (as shown the TG curves in Fig. 6a), which can be attributed to the water evaporation phenomenon. With the heating temperature of increasing to higher than 400°C, the residual weight decreased rapidly with only 10% residue at 700°C. Compared with the pristine cotton, the cotton/pDA shows a similar thermal decomposition behavior due to the amorphous structure of pDA. The residual weight of the cotton/pDA is slightly higher than original cotton. After loading of MnO_2 NPs, however, the TG curve is totally different from either cotton or cotton/pDA. The residual weight of cotton/pDA/MnO_2 is 40.8% higher than cotton/pDA, and it has proven the excellent thermal stability of cotton/pDA/MnO_2. The enhanced thermal stability can be attributed to the enhanced carbonization and invigoration effect of cellulose chain as a result of MnO_2 NPs deposition.

According to DTG curves (Fig. 6b), the maximum thermal degradation temperature (DTG_{max}) of cotton fabric and cotton/pDA is very similar (355°C and 354°C, respectively). This is mainly because the amorphous structure of pDA has little influence on the thermal properties of cotton fibers. For cotton/pDA/MnO_2 sample, the DTG curve has two main weight loss stages occurring over 200 ℃. The first DTG_{max} representing the decomposition of polymers was detected at 233 ℃, which was much lower than the original cotton sample. This is mainly due to the existence of MnO_2 NPs, as the catalytic nanoparticles has reduced the activation energy and accelerated the depolymerization reaction. The second DTG_{max} was at 378 ℃, which was related to phase transition from MnO_2 to Mn_3O_4 by the losing of oxygen from MnO_2 lattice (JCPDS No. 24-0734) (Yang et al. 2021).

3.3 HCHO adsorption property

The HCHO adsorption test of the cotton/pDA/MnO_2 was carried out in a sealed quartz reactor. In the presence of the as-prepared fabrics, the concentration of HCHO decreased from 22.7 ppm to 0 (Fig. 7a). The drop of HCHO concentration is due to the complete absorption of the HCHO by the coated MnO_2 NPs. The experiment was repeated again after the sample had been illuminated by UV lamp for 3h, and it was found that HCHO could be completely adsorbed in about 20 min after three cycles. This result indicates that the cotton/pDA/MnO_2 has good stability for adsorbing HCHO, and the sample can be recycled.

As shown in Fig. 7b, due to the higher concentration of HCHO, the removal efficiency of HCHO gradually increased and the adsorption rate of cotton/pDA/MnO_2 was faster at the initial stage. With the removal of HCHO, the adsorption rate became slower, and finally the HCHO was completely adsorbed in about 20 min.

In order to evaluate the effect of air circulation on the adsorption of HCHO by the cotton/pDA/MnO_2, the parameter of air flowing rate was introduced by turning on a fan mounted on the floor of the reactor. As shown in Fig. 7c, the concentration of HCHO from the 1 mL liquid formaldehyde after gasification was slightly less than 22.7 ppm after adding the fan. This phenomenon is due to the accelerated movement of HCHO molecules that leads to the backflow of HCHO. Obviously, the rate of HCHO adsorption by cotton/pDA/MnO_2 is faster after adding a fan, as the HCHO molecules will move faster to promote absorption.

MnO_2 has been reported as a catalyst for decomposing HCHO. Herein, the efficiency of cotton/pDA/MnO_2 photocatalytic degradation of HCHO under the condition of sunlight and ultraviolet lamp was evaluated by the yield of CO_2 (Fig. 7d). At the initial stage, the concentration of CO_2 was about 1000 ppm due to the presence of CO_2 in the air. Under the irradiation of sunlight and UV lamp, the concentration of CO_2 was increased with the irradiation time, and finally reached the maximum threshold of the detector (5500 ppm). In details, the concentration of CO_2 under sunlight irradiation rose faster and took less time to reach the maximum value than that under UV irradiation. The high solar intensity and temperature (2021.06.24, 3:00 p.m., 36°C, Wuhan, China) of sunlight accelerated the decomposition of HCHO molecules, thus leading to the high efficiency of photocatalytic decomposition of HCHO. On the other hand, the concentration of CO_2 under UV irritation was slow at first and then increased sharply. The temperature in the closed environment was low at the beginning of UV irradiation, resulting in a relatively slow decomposition rate of HCHO molecules. After irradiation for a certain time, the temperature rose and the decomposition of HCHO molecules was accelerated. Overall, cotton/pDA/MnO_2 demonstrated its potential of being used as a catalyst to decompose the adsorbed HCHO into CO_2 under the irradiation of either sunlight or UV lamp.

3.4 Proposed reaction mechanism

A possible reaction mechanism of HCHO removal on the cotton/pDA/MnO_2 is proposed here as shown in Fig. 8. Firstly, the surface of MnO_2 catalyst is oxidized by O_2 in the air to form surface adsorbed oxygen, which then oxidizes HCHO as-adsorbed on the catalyst surface to methylene dioxygen (DOM) (as shown in Eq.) (Lin et al. 2019; Wang et al. 2020). Then, the DOM will be rapidly transformed into formate (HCOO-) species on the cotton/pDA/MnO_2 (as shown in Eq.) (Huang et al. 2021). Finally, the formate species decompose into CO, which further oxidizes into CO_2 (as shown in Eq.) (Sun et al. 2019; Ye et al. 2020). The excellent HCHO oxidation performance of the cotton/pDA/MnO_2 catalyst is mainly due to the following two aspects. First, cotton fabrics have a large specific surface area and porous structure, which is conducive to HCHO diffusion to catalyst surface. Besides, poly(dopamine) is structurally similar to

natural melanin pigment, which can absorb sunlight and facilitate the decomposition of formate species into CO_2. In summary, the cotton/pDA/MnO_2 can adsorb HCHO, and followed by the reutilization.

4. Conclusions

In conclusion, pDA modified cotton fabrics with abundant phenolic hydroxyl groups served as anchoring points for MnO_2 NPs deposition. The SEM, XRD and XPS results have demonstrated that δ-MnO_2 NPs were uniformly dispersed on the surface of cotton fabrics after *in-situ* growth. The HCHO adsorption test results have indicated the excellent catalytic activity cotton/pDA/MnO_2, applicable to effectively adsorb and decompose the HCHO into CO_2 under the irradiation of either sunlight or UV lamp. The HCHO removal efficiency reached to 100% within 20 min after three cycles, suggesting the good stability of the as-prepared fabrics in the degradation of HCHO. The possible reaction mechanism of HCHO removal on the cotton/pDA/MnO_2 was also explored. The high adsorption and degradation efficiency are attributed to the high specific surface area and porous structure of cotton fabrics together with the natural melanin pigment like structure of pDA film. The *in-situ* growth of MnO_2 NPs on pDA-templated cotton fabrics is a promising strategy to solve the increasingly urgent problem of HCHO in interior decorations.

Declarations

Acknowledgement

This research was supported by the Key Project of the EducationDepartmentof Hubei Province (D20211702) and the Key Laboratory of Fujian Provincial Key Labof Coastal Basin Environment, Fujian Polytechnic Normal University (S1-KF2005).

References

1. AbduH, KinfuY, AgaluA(2014)Toxic effects of formaldehyde on the nervous system.IntJAnatPhysiol3:50-59.
2. BaiB, QiaoQ, LiJ, HaoJ(2016)Progress in research on catalysts for catalytic oxidation of formaldehyde.Chinese JCatal37(1):102-122.
3. ChenX, GaoP, GuoL, WenY, FangD, GongB,ZhangS(2017a)High-efficient physical adsorption and detection of formaldehyde using Sc-and Ti-decorated graphdiyne.PhysLettA381(9):879-885.
4. ChenLY, LinMW, ChuahYK(2017b)Investigation of a potted plant (Hedera helix) with photo-regulation to remove volatile formaldehyde for improving indoor air quality.AerosolAir QualRes17(10):2543-2554.
5. ChengD, HeM, RanJ, CaiG, WuJ,WangX(2018)In situ reduction of TiO_2 nanoparticles on cotton fabrics through polydopamine templates for photocatalysis and UV protection.Cellulose25(2):1413-1424.
6. ChengD, BaiX, PanJ, WuJ, RanJ, CaiG,WangX(2020)In situ hydrothermal growth of CuNPs on knitted fabrics through polydopamine templates for heating and sensing.ChemEngJ382:123036-123045.

7. ChengD, LiuY, YanC, ZhouY, DengZ, RanJ,WangX(2021)WPU/Cu_{2-X}Se coated cotton fabrics for photothermal conversion and photochromic applications.Cellulose28:6727-6738.
8. DaiZ, ZhuJ, YanJ, SuJ, GaoY, ZhangX,ParsonsGN(2020)An Advanced Dual-Function MnO2-Fabric Air Filter Combining Catalytic Oxidation of Formaldehyde and High-Efficiency Fine Particulate Matter Removal.AdvFunctMater30(42):2001488-2001499.
9. FalcoG, LiW, CiminoS, BandoszTJ(2018)Role of sulfur and nitrogen surface groups in adsorption of formaldehyde on nanoporous carbons.Carbon138:283-291.
10. French AD, Cintrón MS (2013) Cellulose polymorphy, crystallite size, and the Segal crystallinity index. Cellulose 20(1):583-588.
11. French AD (2014) Idealized powder diffraction patterns for cellulose polymorphs. Cellulose 21(2):885-896.
12. HuangS, ZhuX, ChengB, YuJ,JiangC(2017)Flexible nickel foam decorated with Pt/NiO nanoflakes with oxygen vacancies for enhanced catalytic formaldehyde oxidation at room temperature.EnvironSci Nano4(11):2215-2224.
13. İnciM, Zararsızİ, DavarcıM, GörürS(2013)Toxic effects of formaldehyde on the urinary system.Turk JUrol39(1):48-52.
14. JiJ, LuX, ChenC, HeM,HuangH(2020)Potassium-modulated δ-MnO_2 as robust catalysts for formaldehyde oxidation at room temperature.ApplCatalBEnviron260:118210-118221.
15. KimKH, JahanSA, LeeJT(2011)Exposure to formaldehyde and its potential human health hazards.JEnvironSciHeal C 29(4):277-299.
16. LiZ, MiY, LiuX, LiuS, YangS,WangJ(2011)Flexible graphene/MnO_2 composite papers for supercapacitor electrodes.JMaterChem21(38):14706-14711.
17. LinM, YuX, YangX, MaX,GeM(2019)Exploration of the active phase of the hydrotalcite-derived cobalt catalyst for HCHO oxidation.Chinese JCatal40(5):703-712.
18. LuL, TianH, HeJ,YangQ(2016)Graphene-MnO_2 hybrid nanostructure as a new catalyst for formaldehyde oxidation.JPhysChemC120(41): 23660-23668.
19. LuWJ, HuangSZ, MiaoL, LiuMX, ZhuDZ, LiLC,GanLH(2017)Synthesis of MnO_2/N-doped ultramicroporous carbon nanospheres for high-performance supercapacitor electrodes.ChinChemLett28(6):1324-1329.
20. MaL, MengN, ZhangY,LianF(2019)Improved electrocatalytic activity of δ-MnO_2@MWCNTs by inducing the oriented growth of oxygen reduction products in Li-O_2 batteries.Nano Energy58:508-516.
21. MiaoY, FengY, BaiJ, LiuZ,ZhaoX(2021)Optimized mesoporous silica nanoparticle-based drug delivery system with removable manganese oxide gatekeeper for controlled delivery of doxorubicin.JColloidInterfSci592:227-236.
22. NieL, YuJ, JaroniecM, TaoFF(2016)Room-temperature catalytic oxidation of formaldehyde on catalysts.CatalSciTechnol6(11):3649-3669.

23. QiQ, ZhangW, ZhangY, BaiG, WangS,LiangP(2021)Formaldehyde oxidation at room temperature over layered MnO_2.CatalCommun153:106293-106297.
24. Quiroz TJ, RoyerS, BellatJP, GiraudonJM, LamonierJF(2013)Formaldehyde: catalytic oxidation as a promising soft way of elimination.ChemSusChem6(4):578-592.
25. RanJ, BiS, JiangH, TeleginF, BaiX, YangH,WangX(2019)Core-shell $BiVO_4$@PDA composite photocatalysts on cotton fabrics for highly efficient photodegradation under visible light.Cellulose26(10):6259-6273.
26. RanJ, ChenH, BiS, GuoQ, YanC, TangX,WangX(2021)Polydopamine-induced in-situ growth of zeolitic imidazolate framework-8/TiO_2 nanoparticles on cotton fabrics for photocatalytic performance.ProgOrgCoat152:106123-106131.
27. RongS, ZhangP, LiuF,YangY(2018)Engineering crystal facet of α-MnO_2 nanowire for highly efficient catalytic oxidation of carcinogenic airborne formaldehyde.ACSCatal8(4):3435-3446.
28. ShiX, LiY, ChenR, NiH, ZhanW, ZhangB,DongS(2018)Defective carbon nanotube forest grown on stainless steel encapsulated in MnO_2 nanosheets for supercapacitors.ElectrochimActa278:61-71.
29. SunD, WagehS, Al-GhamdiAA, LeY, YuJ,JiangC(2019)Pt/C@MnO_2 composite hierarchical hollow microspheres for catalytic formaldehyde decomposition at room temperature.ApplSurfSci466:301-308.
30. WangM, ZhangG, QiuG, CaiD,WuZ(2016)Degradation of herbicide (glyphosate) using sunlight-sensitive MnO_2/C catalyst immediately fabricated by high energy electron beam.ChemEngJ306:693-703.
31. WangJ, LiJ, JiangC, ZhouP, ZhangP,YuJ(2017)The effect of manganese vacancy in birnessite-type MnO_2 on room-temperature oxidation of formaldehyde in air.ApplCatalBEnviron204:147-155.
32. WangZ, ChengY, YangM, HuangJ, CaoD, ChenS,WuH(2018)Dielectric properties and thermal conductivity of epoxy composites using core/shell structured Si/SiO_2/Polydopamine.ComposBEng140:83-90.
33. WangC, ChenT, LiuH, XieJ, LiM, HanZ,SuibSL(2019)Promotional catalytic oxidation of airborne Formaldehyde over mineral-supported MnO_2 at ambient temperature.ApplClay Sci182:105289-105300.
34. WangY, LiuK, WuJ, HuZ, HuangL, ZhouJ,GuoL(2020)Unveiling the effects of alkali metal ions intercalated in layered MnO_2 for formaldehyde catalytic oxidation.ACS Catal10(17):10021-10031.
35. YangJ, AoZ, WuH,ZhangS(2021)Immobilization of chitosan-templated MnO_2 nanoparticles onto filter paper by redox method as a retrievable Fenton-like dip catalyst.Chemosphere268:128835-128843.
36. YeJ, ZhouM, LeY, ChengB,YuJ(2020)Three-dimensional carbon foam supported MnO_2/Pt for rapid capture and catalytic oxidation of formaldehyde at room temperature.ApplCatalBEnviron267:118689-118696.

37. Zhang H, Cao D, Bai X (2019) High rate performance of aqueous magnesium-ion batteries based on the δ-MnO_2@ carbon molecular sieves composite as the cathode and nanowire VO_2 as the anode. J Power Sources 444:227299-2273006.
38. ZhuB, LiXS, SunP, LiuJL, MaXY, ZhuX, ZhuAM(2017a)A novel process of ozone catalytic oxidation for low concentration formaldehyde removal.Chinese JCatal38(10):1759-1769.
39. ZhuL, WangJ, RongS, WangH, ZhangP(2017b)Cerium modified birnessite-type MnO_2 for gaseous formaldehyde oxidation at low temperature.ApplCatalBEnviron211:212-221.

Figures

Figure 1

The preparation process ofMnO_2 NPs coated cotton fabricsvia *insitu* growth.

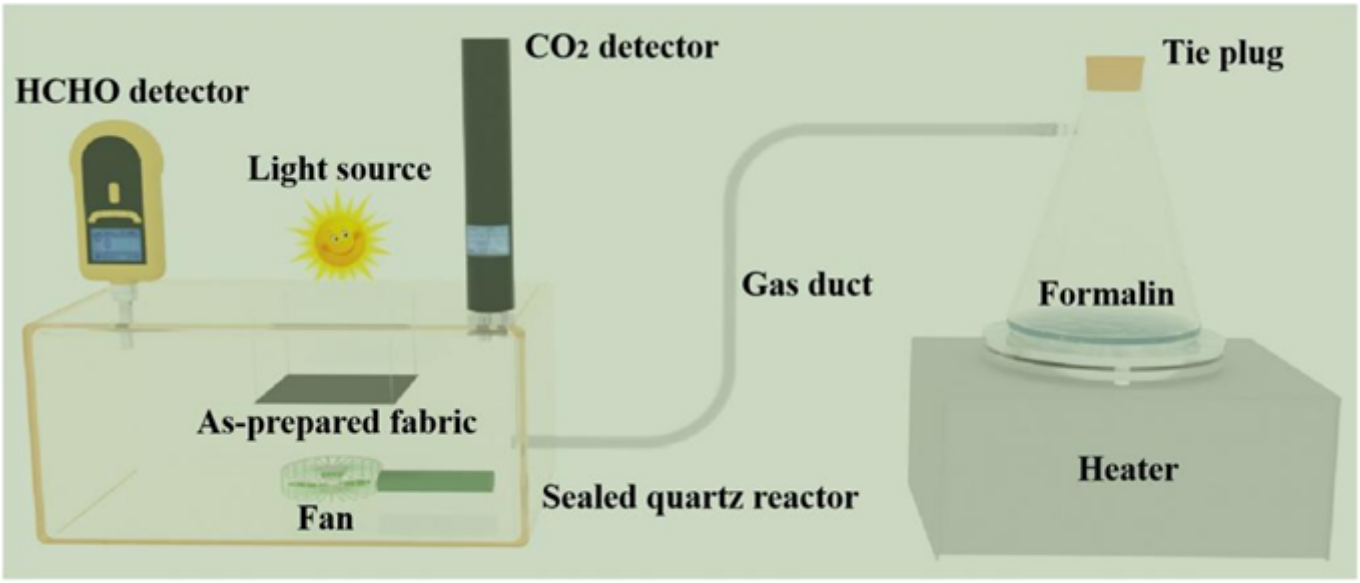

Figure 2

Schematics of HCHO adsorption test.

Figure 3

SEM images of pristine cotton (a), cotton/pDA (b), and cotton/pDA/MnO_2 with different resolutions (c-d) (Insets: optical photos of corresponding samples); SEM-EDS elemental map of Mn (e), and EDS patterns collected from the cotton/pDA/MnO_2 (f).

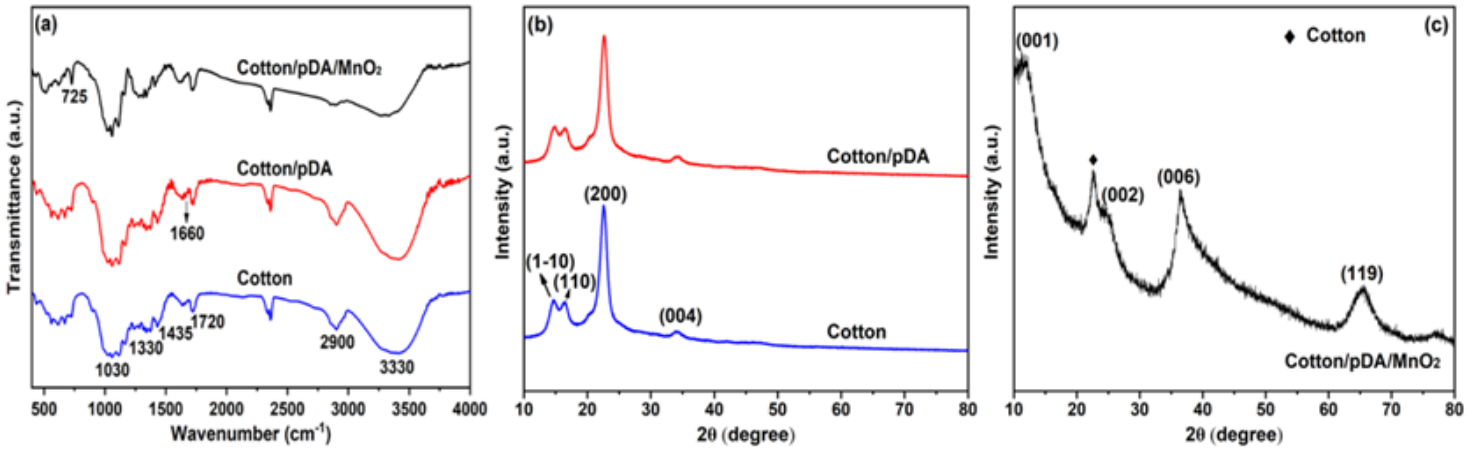

Figure 4

FTIR (a) and XRD (b-c) pattern of pristine cotton, cotton/pDA, and cotton/pDA/MnO_2.

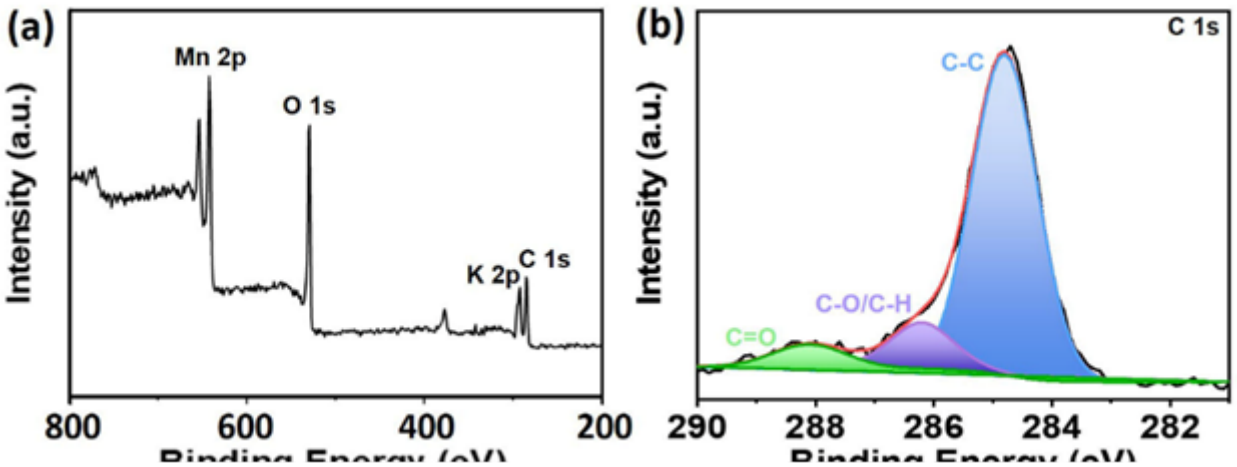

Figure 5

The survey XPS spectra of cotton/pDA/MnO_2 (a) and high resolutionof C 1s, Mn 2p, and O 1s peak (b-d).

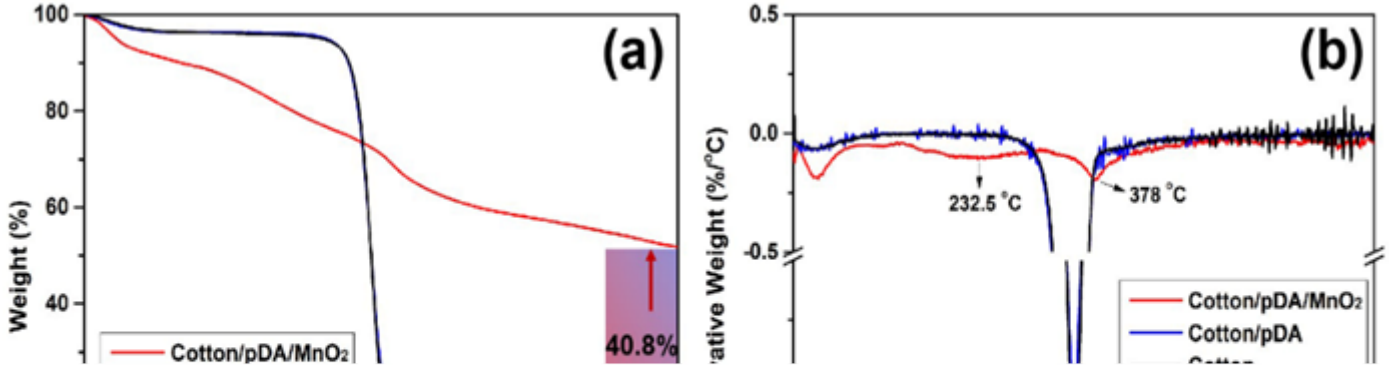

Figure 6

TG curves (a) and derivative weight (b) of cotton, cotton/pDA, and cotton/pDA/MnO_2.

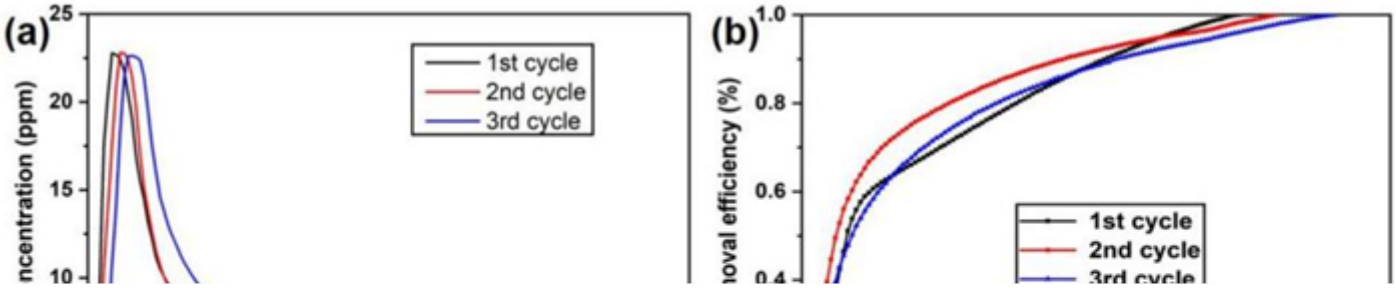

Figure 7

The concentration of HCHO in the adsorption process in repeated 3 cycle (a), the removal efficiency in each HCHO adsorption test (b), effect of cotton/pDA/MnO_2 on HCHO adsorption before and after the fan was turned on(c) and effect of UV lamp and sunlight on oxidation of HCHO into CO_2(d).

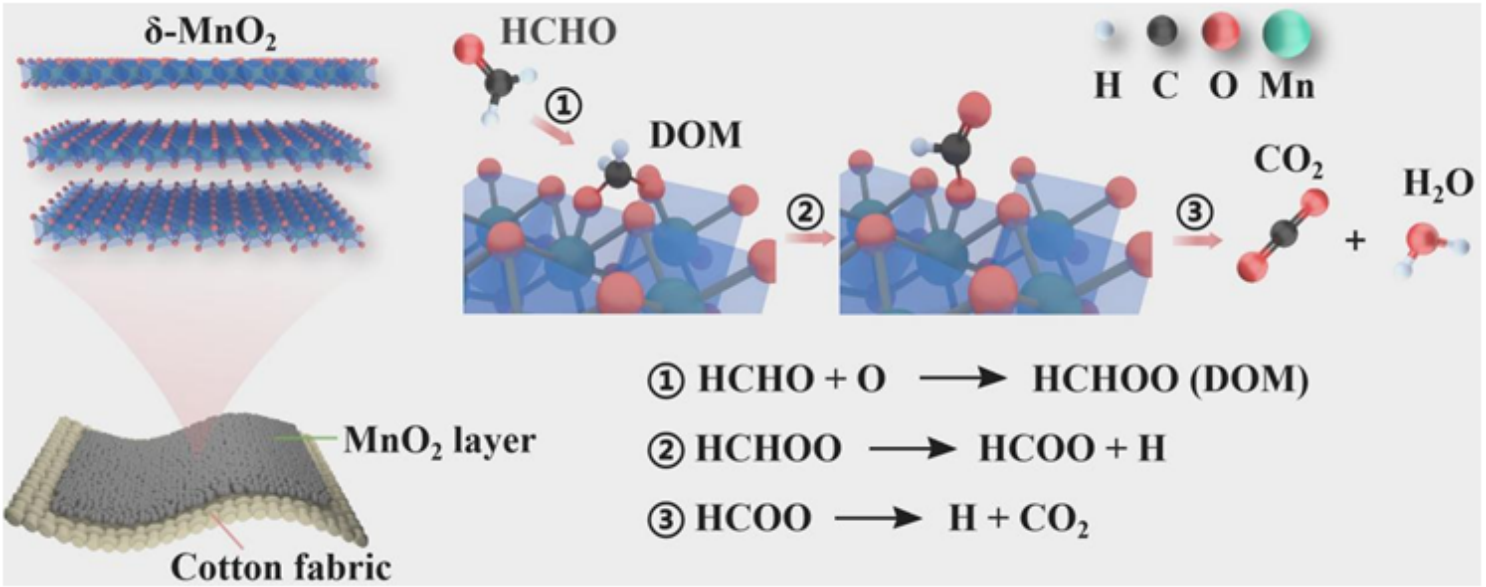

Figure 8

Proposed reaction mechanism of HCHO removalon the cotton/pDA/MnO2.